Fourier Transform Acousto-Optic Imaging with a custom-designed CMOS smart-pixels array

Kinia Barjean, Kevin Contreras, Jean-Baptiste Laudereau, Éric Tinet, Dominique Ettori, François Ramaz, Jean-Michel Tualle

Fourier Transform Acousto-Optic Imaging with a custom-designed CMOS smart-pixels array

Kinia Barjean,[1] Kevin Contreras,[2] Jean-Baptiste Laudereau,[2] Éric Tinet,[1] Dominique Ettori,[1] François Ramaz,[2] and Jean-Michel Tualle[1,*]

[1] *Laboratoire de Physique des lasers, CNRS UMR 7538, Université Paris Nord 13, 99 Ave J.B. Clément, F-93430 Villetaneuse, France*

[2] *Institut Langevin, Ondes et Images, ESPCI ParisTech, PSL Research University, CNRS UMR 7587, INSERM U979, Université Paris VI-Pierre et Marie Curie, 1 rue Jussieu, 75005 Paris, France*

compiled: November 14, 2014

We report acousto-optic imaging (AOI) into a scattering medium using a Fourier Transform (FT) analysis to achieve axial resolution. The measurement system was implemented using a CMOS smart-pixels sensor dedicated to the real-time analysis of speckle patterns. This first proof-of-principle of FT-AOI demonstrates some of its potential advantages, with a signal to noise ratio comparable to the one obtained without axial resolution, and with an acquisition rate compatible with a use on living biological tissue.

OCIS codes: 110.0113,110.7170,170.3880,170.3660,250.3140

Acousto-optic imaging (AOI) is an emerging technique in the field of biomedical optics, which couples light and ultrasound. It enables access to the contrast allowed by diffuse optical tomography [1, 2] with the resolution of ultrasound (US) imaging [3]. When propagating through an illuminated area, US modulate the refractive index and the scattering particles motion at the US frequency. It results in the creation of optical sidebands in the scattered light spectrum, shifted of the US wave frequency [4]. The amount of frequency-shifted photons, the so-called tagged-photons, is proportional to the local light irradiance, and filtering them allows recovering relevant optical information [5].

Here the frequency shifts considered (a few MHz) are very small compared to light frequency (few hundreds THz). Although high finesse spectral filters, using spectral hole-burning at cryogenic temperatures, have proven their ability to discriminate the tagged photons [6], a lot of groups are currently focusing on interferometric detection schemes which, for now, seem to be more accessible for medical applications [7–11].

Interferometric methods present the advantage of moving the frequency shifts into more accessible regions for classical detectors. Of course one has to manage the limited spatial coherence of diffuse light, which appears as a speckle pattern. Thanks to photorefractive crystals, self-adaptive holography can deal with such spatially incoherent wavefronts [7, 8]. However this technique is still not validated with living tissue due to the response time of photorefractive crystals (millisecond range), which is somewhat limited compared to the short correlation time of the speckle pattern (submillisecond range for living tissue [12]). And even if this problem could be solved in the near future, this technology is not as widespread as CMOS sensors.

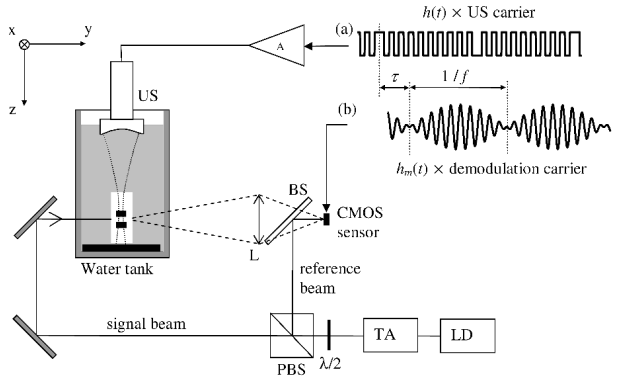

Fig. 1. Experimental setup. LD: laser diode; TA: tapered amplifier; PBS: polarization beam splitter; L: imaging lens; BS: low reflectivity beam splitter; A: RF amplifier; (a) control signal for US generation; (b) demodulation signal for the lock-in detection.

High acquisition rate pixel array sensors enable spatio-temporal sampling of the speckle pattern. Therefore

* Corresponding author: tualle@univ-paris13.fr

they deal with both incoherent wavefronts and fast speckle decorrelation. Off-axis digital holography [10] currently exploits such devices, whose main drawbacks are the cost and the data transfer delay.

In this work we have implemented a fast CMOS sensor dedicated to the real-time analysis of speckle patterns [13]. We implemented this sensor with a low-cost technology, which could be an asset for a wide distribution of this diagnostic tool. We used this sensor to validate a new method to achieve axial resolution along the US beam propagation axis (z-axis in figure 1) through a Fourier Transform analysis. In this letter we present this method as a proof-of-principle, with a brief derivation.

Actually, the only way to allow axial resolution is to modulate the US source by a function of time $h(t)$, in order to 'tag' the US wave at position z by a factor $h(t+\tau-u^{-1}z)$, where τ is a delay and u the US velocity in the medium ($u = 1.5mm/\mu s$ in water). The interferometric signal depends linearly on the electromagnetic field, and accordingly it depends linearly on the amplitude of the US wave pressure and on the modulation h [14]. In order to decode the position information, one can therefore multiply the interferometric signal by a demodulation function $h_m(t)$ before time averaging on the detector: such an operation is equivalent to the introduction of a 'virtual' weighting factor which is the correlation function [15]:

$$g(u^{-1}z-\tau) = \langle h(t+\tau-u^{-1}z)h_m(t)\rangle_T, \qquad (1)$$

where $\langle\cdots\rangle$ denotes a time average (t variable) over the integration time T of the detector. We have to square the signal recorded at each pixel in order to recover, through an ensemble averaging over all pixels, a measured signal φ_{tag} proportional to the radiant flux of the tagged photons at the detector level. As this tagged flux depends on the square of the amplitude of the US wave pressure [14], the weighting factor for the tagged photons radiant flux will therefore be $g^2(z/u-\tau)$, so that:

$$\varphi_{tag} = \int g^2(u^{-1}z-\tau)S(z)dz, \qquad (2)$$

where the integration is performed along the US beam and where $S(z)$ is proportional to: the local irradiance, the tagging efficiency, and the Green function accounting for propagation from the tagging position to the detector.

Different choices can be considered for the above-mentioned functions. First, in the simplest case of a continuous US wave (CW), corresponding to $h = h_m = 1 = g^2$, there is no axial resolution and every position z in the region illuminated by diffuse light will contribute to the φ_{tag}. As a consequence the latter will be of the order of

$$\varphi_0 \approx W\bar{S}, \qquad (3)$$

where W is the typical size of the illuminated zone, and $\bar{S}$ a typical value for S.

A choice to allow axial resolution is a pulse of width $\delta t = \delta z/u$ for $h = h_m$. In that case the function g^2 will act as a gate of height $g^2_{max} = (\delta t/T)^2 = (\delta z/L)^2$, where $L = uT$ is the distance travelled by the US beam during the integration time T, and where δz is the axial resolution. In fact, the choice of a pulse for h_m implies a reduction of the integration time, and thus of the corresponding integrated signal, what explains this huge reduction of g^2 compared to the previous CW case.

Compared to the choice of a US pulse, the method of random phase jumps [14] presents the advantage of exploiting the whole integration time: the function $h = h_m$ is randomly drawn after each period $\delta t = \delta z/u$ to be $+1$ or -1 with equal probability. The function g^2 is now a gate of unit height and axial resolution δz, over a random background of order $\delta z/L$. This method corresponds to a great improvement compared to the choice of a pulse [10], even if there is still a reduction of the signal to noise ratio (SNR) when compared to the CW case (Eq. 3): the signal, of order $\bar{S}\delta z$, is indeed lowered by a factor $\delta z/W$ due to the limited area selected by the gate g^2 in Eq. 2. Furthermore, random phase jumps usually imply integration times of several hundreds microseconds [10], what can be problematic for biomedical applications.

In the present paper, we propose to choose h as a periodic square function, oscillating between $+1$ and -1 at a frequency $f/2$, and to choose $h_m = \sin(\pi f t)$ so that one has for the choice of a delay $\tau = \theta/(\pi f)$:

$$g^2(u^{-1}z-\tau) = \kappa\cos^2(\pi\nu z-\theta), \qquad (4)$$

with $\kappa = 4/\pi^2$ and where $\nu = f/u$ is the spatial frequency corresponding to f. If $\varphi_{tag}(\nu;\theta)$ is the tagged signal measured with such a choice, one only has to compute, in order to have the Fourier transform of S at a spatial frequency ν:

$$\begin{aligned}\kappa\tilde{S}(\nu) \equiv\ & \varphi_{tag}(\nu;0) - \varphi_{tag}(\nu;\tfrac{\pi}{2}) \\ & + j\varphi_{tag}(\nu;-\tfrac{\pi}{4}) - j\varphi_{tag}(\nu;\tfrac{\pi}{4})\end{aligned} \qquad (5)$$

Within the framework of Discrete Fourier Transform (DFT), one has to record $N = L/\delta z$ values for frequencies $\nu_n = n/L$ and to apply inverse DFT in order to obtain $\kappa S(z)\delta z$ at points $z = m\delta z$. The signal here is in the same range as the one obtained with the method of random phase jumps, but on the other hand the noise should be divided by a factor $\sqrt{N}$ after the DFT due to the $1/N$ term in the definition of the inverse DFT. So one can expect a higher SNR with this method.

The above-mentioned concepts were experimentally validated using the setup depicted in Fig. 1. The light source consists in a single-frequency semi-conductor laser diode (LD) emitting at $790nm$, amplified with a $2W$ tapered amplifier (TA, Sacher laser technik - GmbH). A small part of the laser beam is sent towards

the CMOS sensor as a reference beam, through a low-reflectivity beamsplitter (BS, reflectivity of 5% allowing an irradiance of $40mW/cm^2$ on the sensor). The sample is placed into a Plexiglas water tank for acoustical contact. The incident beam on the sample has a power of about $1W$. The transmitted light is collected by a lens (L) and interferes with the reference beam on the sensor.

The CMOS sensor was a 24×24 pixels prototype [13] with a surface of $1mm^2$. For each pixel independently, this circuit has the ability to perform a lock-in detection of the beat at the US frequency between the tagged beam and the reference beam through the multiplication by a demodulation signal. Simultaneously, by tuning this demodulation signal, the circuit can perform the multiplication by the function h_m needed in the present protocol. The outputs of the lock-in detections are then squared and averaged over all pixels in order to recover a radiant flux. This average value is the only output of the sensor, so that high acquisition rate can be achieved (3600 frames/s in the present case).

The US beam is generated by an acoustic transducer (Panametrics $A395S-SU$) with a focal length of $75mm$. The beam has a frequency of $2.3MHz$ and is focused on the sample, with a US pressure of the order of $1MPa$ at the focal point. In the present experiment, the transducer is controlled by a two-state signal which encodes both the US carrier at $2.3MHz$ and the modulation function h (see Fig.1). The demodulation signal sent to the sensor lock-in detection includes for its part both the demodulation carrier and the function h_m (see Fig.1). The demodulated signal is integrated over a time $T = 70\mu s$, what corresponds to a length $L = 10.5cm$ greater than the depth of the water tank. Each measurement is averaged over 5000 frames. At a rate of 3600 frames/s, $5.5s$ are therefore needed to acquire all the components of Eq.5. We choose to split the length L into $N = 60$ intervals, so that $N/2 = 30$ Fourier components have to be measured in order to reconstruct $S(z)$. This corresponds to a spatial resolution $\delta z = L/N = 1.75mm$ (let us note that, strictly speaking, the full width at half maximum -FWHM- of the point spread function is rather $2.1mm$).

The sample was a $2 \times 4 \times 4cm^3$ gel matrix ($2cm$ thick along the light propagation axis y) constituted with an agar gel mixed intralipid 10%. The concentration of intralipid is adjusted to obtain a reduced scattering coefficient of about $10cm^{-1}$. Agar is diluted into hot water at $90°C$ and intralipid is added once the mixture has cooled down $70°C$ or less. Two cylindrical inclusions with addition of India ink ($3mm$ diameter, $5mm$ length) were placed in the middle of the sample. They are separated by a distance of $3mm$ along the z-axis in order to test the ability of FT-AOI to perform axial resolution. The acoustic transducer is mounted on a translation stage in order to move it along the x-axis.

Let us first consider measurements performed outside the inclusions: in that case the tagged signal mainly probes the distribution of diffuse light within the medium. At low modulation frequencies f, the acquisition is somewhat equivalent to the CW case as we mainly measure the integral of $S(z)$. In the present experiment we measure for the CW case (Eq. 3) a signal of $\varphi_0 = 18mV$ for a noise of about $1mV$, with a resulting SNR of 18 (let us recall that this value corresponds to a measured voltage, and is directly proportional to the tagged flux). To account for bandwidth limitations in the setup, the first three Fourier components were multiplied by fixed pre-calibrated coefficients (of modules 1.2, 0.9 and 0.95) determined from previous experiments.

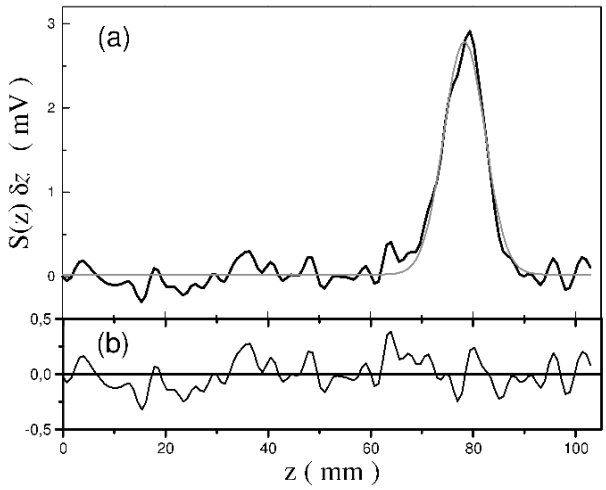

Fig. 2. (a): Axial profile (solid black) measured by FT-AOI with a scattering medium in the water tank. Measurements are performed outside the inclusions, and the signal corresponds to the distribution of diffuse light, with an expected Gaussian shape (Gaussian fit in solid gray). (b) Residual error (difference between the signal and the fit, in mV).

The inverse DFT of the recorded Fourier components is presented on Fig.2a as a function of the z-axis position (with a Shannon interpolation between the sampling points). The signal is maximal at a depth of about $8cm$ from the transducer, what corresponds to the position of the sample. The shape is well fitted by a Gaussian with a FWHM of $W = 9.5mm$, in good agreement with what should be expected from diffusion theory. Let us recall that the inverse DFT is $S(z)$ times δz: the typical value expected for $\bar{S}$ using Eq. 3 should be $\varphi_0/W \approx 2mV/mm$, so that the value $\bar{S}\delta z \approx 3mV$ is in good agreement with the typical values of the Fig.2a. The residual noise obtained with the difference between the signal and the Gaussian fit is presented in Fig.2b: the standard deviation is $0.14mV$, what is in good agreement with a noise of $1mV$ in the Fourier components divided by $\sqrt{N}$. Finally, this gives a SNR of ≈ 22. In this example, we therefore have a higher SNR with axial resolution rather than without: this is due to the fact that $L > W$, what implies an averaging linked to super-abundant measurements. Anyway, this underlines the SNR performance of the method.

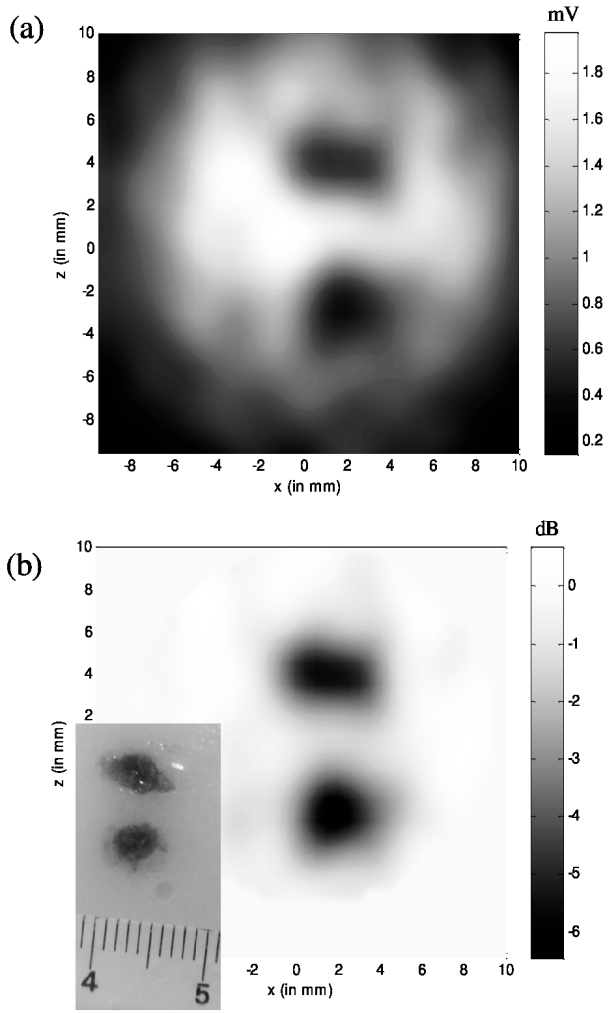

Fig. 3. (a) Acousto-optic image obtained by gathering z-scans at different positions x of the acoustic transducer; (b) Ratio between the acousto-optic image and the fitted Gaussian envelop accounting for non-uniform illumination; the inset is a picture of the sample just after the implementation of the cylindrical inclusions.

In order to demonstrate the ability of the method to perform imaging, we achieve an x-z image of the two absorbing inclusions placed within the medium. In order to increase the size of the illuminated region, a piece of translucent tape was fixed on the input wall of the water tank, a few centimeters before the sample: the incident laser light is slightly scattered and its size on the sample is slightly increased (up to about 1 cm^2). We record z-scans of the sample at different positions along the x-axis, within an interval of $2cm$ and with a fixed step of $0.5mm$. In order to have the same spatial resolution in the x and z directions, the obtained image was filtered in the x direction with the same spatial cut-off frequency as for the z-scan ($k_c \equiv 2\pi\nu_c \approx 1.9mm^{-1}$). This image, presented in Fig. 3a, is clearly affected by the non-uniform illumination. In order to remove the effect of non-uniform illumination and to exhibit the absorption properties of the inclusions, the scattering envelop was fitted by a Gaussian, and we calculated the ratio between the acousto-optic image and the fitted envelope: this ratio, expressed in dB, is plotted in Fig. 3b. These images can be compared to a picture of the inclusion taken just after their implementation, and before being covered by an additional layer of scattering gel. The inclusions are clearly resolved, illustrating the potential spatial resolution of the method.

In conclusion, we have introduced and demonstrated experimentally a new method to perform axial resolution in acousto-optic imaging. In comparison to existing techniques in this field, this method should allow a consequent improvement of the signal to noise ratio (SNR). The results were obtained using an innovative CMOS smart-pixels sensor with an integration time ($70\mu s$) compatible with typical correlation times observed with living biological tissue. For this proof of principle the setup has not been optimized, and we expect a far better SNR in the near future: for instance, we used a small-size prototype ($1mm^2$) for the CMOS sensor, and the SNR should be considerably increased (factor 10) with a sensor of usual size, in the range of $1cm^2$.

This work was supported by the French National Research Agency (project ANR-11-BS04-0017, ICLM).

References

[1] A. P. Gibson, J. C. Hebden, and S. R. Arridge, Phys. Med. Biol. **50**, R1 (2005).
[2] P. Taroni, A. Pifferi, E. Salvagnini, L. Spinelli, A. Torricelli, and R. Cubeddu, Opt. Express **17**, 15932 (2009).
[3] F. A. Marks, H. W. Tomlinson, and G. W. Brooksby, Proc. SPIE **1888**, 500 (1993).
[4] W. Leutz and G. Maret, Physica B **204**, 14 (1995).
[5] J.-B. Laudereau, E. Benoit La Guillaume, V. Servois, P. Mariani, A. A. Grabar, M. Tanter, J.-L. Gennisson, and F. Ramaz, J. Biophot. **DOI** 10.1002/jbio.201400071 (2014).
[6] Y. Li, H. Zhang, C. Kim, K. H. Wagner, P. Hemmer, and L. V. Wang, Appl. Phys. Lett. **93**, 011111 (2008).
[7] T.W. Murray, L. Sui, G. Maguluri, R.A. Roy, A. Nieva, F. Blonigen, and C.A. DiMarzio, Opt. Lett. **29**, 2509 (2004).
[8] F. Ramaz, B.C. Forget, M. Gross, M. Atlan, P. Delaye, G. Roosen, A.C. Boccara, Opt. Exp. **12** pp. 5469 (2004).
[9] M. Atlan, B. C. Forget, F. Ramaz, A. C. Boccara and M. Gross, Opt. Lett. **30**, 1360 (2005).
[10] E. Benoit a la Guillaume, S. Farahi, E. Bossy, M. Gross, and F. Ramaz, Opt. Lett. **37**, 3216 (2012).
[11] D.S. Elson, R. Li, C. Dunsby, R. Eckersley and M.-X. Tang, Interface Focus **1**, 632 (2011).
[12] M. Gross, P. Goy, B. C. Forget, M. Atlan, F. Ramaz, A. C. Boccara, A. K. Dunn, Opt. Lett. **30**, 1357 (2005).
[13] J.-M. Tualle, A. Dupret, M. Vasiliu, Electr. Lett. **46**, 819 (2010).
[14] M. Lesaffre, S. Farahi, A. C. Boccara, F. Ramaz, and M. Gross, JOSA A **28**, 1436 (2011).
[15] K. Zarychta, E. Tinet, L. Azizi, S. Avrillier, D. Ettori, and J.-M. Tualle, Opt. Exp. **18**, 16289 (2010).

References

[1] A. P. Gibson, J. C. Hebden, and S. R. Arridge, *Recent advances in diffuse optical imaging*, Phys. Med. Biol. **50**, R1 (2005).

[2] P. Taroni, A. Pifferi, E. Salvagnini, L. Spinelli, A. Torricelli, and R. Cubeddu, *Seven-wavelength time-resolved optical mammography extending beyond 1000 nm for breast collagen quantification*, Opt. Express **17**, 15932 (2009).

[3] F. A. Marks, H. W. Tomlinson, and G. W. Brooksby, *Comprehensive approach to breast cancer detection using light: photon localization by ultrasound modulation and tissue characterization by spectral discrimination*, Proc. SPIE **1888**, 500 (1993).

[4] W. Leutz and G. Maret, *Ultrasonic modulation of multiply scattered light*, Physica B **204**, 14 (1995).

[5] J.-B. Laudereau, E. Benoit La Guillaume, V. Servois, P. Mariani, A. A. Grabar, M. Tanter, J.-L. Gennisson, and F. Ramaz, *Multi-modal acousto-optic/ultrasound imaging of ex vivo liver tumors at* 790 *nm using a* $Sn_2P_2S_6$ *wavefront adaptive holographic setup*, J. Biophot. **DOI** 10.1002/jbio.201400071 (2014).

[6] Y. Li, H. Zhang, C. Kim, K. H. Wagner, P. Hemmer, and L. V. Wang, *Pulsed ultrasound-modulated optical tomography using spectral-hole burning as a narrowband spectral filter*, Appl. Phys. Lett. **93**, 011111 (2008).

[7] T.W. Murray, L. Sui, G. Maguluri, R.A. Roy, A. Nieva, F. Blonigen, and C.A. DiMarzio, *Detection of ultrasound-modulated photons in diffuse media using the photorefractive effect*, Opt. Lett. **29**, 2509 (2004).

[8] F. Ramaz, B.C. Forget, M. Gross, M. Atlan, P. Delaye, G. Roosen, A.C. Boccara, *Photorefractive detection of tagged photons in ultrasound modulated optical tomography of thick biological tissues*, Opt. Exp. **12** pp. 5469 (2004).

[9] M. Atlan, B. C. Forget, F. Ramaz, A. C. Boccara and M. Gross, *Pulsed acousto-optic imaging in dynamic scattering media with heterodyne parallel speckle detection*, Opt. Lett. **30**, 1360 (2005).

[10] E. Benoit a la Guillaume, S. Farahi, E. Bossy, M. Gross, and F. Ramaz, *Acousto-optical coherence tomography with a digital holographic detection scheme*, Opt. Lett. **37**, 3216 (2012).

[11] D.S. Elson, R. Li, C. Dunsby, R. Eckersley and M.-X. Tang, *Ultrasound-mediated optical tomography: a review of current methods*, Interface Focus **1**, 632 (2011).

[12] M. Gross, P. Goy, B. C. Forget, M. Atlan, F. Ramaz, A. C. Boccara, A. K. Dunn, *Heterodyne detection of multiply scattered monochromatic light with a multipixel detector*, Opt. Lett. **30**, 1357 (2005).

[13] J.-M. Tualle, A. Dupret, M. Vasiliu, *Ultra-compact sensor for diffuse correlation spectroscopy*, Electr. Lett. **46**, 819 (2010).

[14] M. Lesaffre, S. Farahi, A. C. Boccara, F. Ramaz, and M. Gross, *Theoretical study of acousto-optical coherence tomography using random phase jumps on ultrasound and light*, JOSA A **28**, 1436 (2011).

[15] K. Zarychta, E. Tinet, L. Azizi, S. Avrillier, D. Ettori, and J.-M. Tualle, *Time-resolved diffusing wave spectroscopy with a CCD camera*, Opt. Exp. **18**, 16289 (2010).